OXFORD

Human Molecular Genetics, 2017, Vol. 26, No. 11 2018–2033

doi: 10.1093/hmg/ddx083
Advance Access Publication Date: 7 March 2017
Original Article

ORIGINAL ARTICLE

Impaired fetal muscle development and JAK-STAT activation mark disease onset and progression in a mouse model for merosin-deficient congenital muscular dystrophy

Andreia M. Nunes[1,2], Ryan D. Wuebbles[2,†], Apurva Sarathy[2,†], Tatiana M. Fontelonga[2], Marianne Deries[1], Dean J. Burkin[2] and Sólveig Thorsteinsdóttir[1,3,*]

[1]Departamento de Biologia Animal, Centro de Ecologia, Evolução e Alterações Ambientais, Faculdade de Ciências, Universidade de Lisboa, 1749-016 Lisbon, Portugal, [2]Center for Molecular Medicine, University of Nevada School of Medicine, Reno, NV 89557, USA and [3]Instituto Gulbenkian de Ciência, 2780-156 Oeiras, Portugal

*To whom correspondence should be addressed. Tel: +351 217500212; Fax: +351 217500028; Email: solveig@fc.ul.pt

Abstract

Merosin-deficient congenital muscular dystrophy type 1A (MDC1A) is a dramatic neuromuscular disease in which crippling muscle weakness is evident from birth. Here, we use the dy^{W} mouse model for human MDC1A to trace the onset of the disease during development *in utero*. We find that myotomal and primary myogenesis proceed normally in homozygous $dy^{W-/-}$ embryos. Fetal $dy^{W-/-}$ muscles display the same number of myofibers as wildtype (WT) muscles, but by E18.5 $dy^{W-/-}$ muscles are significantly smaller and muscle size is not recovered post-natally. These results suggest that fetal $dy^{W-/-}$ myofibers fail to grow at the same rate as WT myofibers. Consistent with this hypothesis between E17.5 and E18.5 $dy^{W-/-}$ muscles display a dramatic drop in the number of Pax7- and myogenin-positive cells relative to WT muscles, suggesting that $dy^{W-/-}$ muscles fail to generate enough muscle cells to sustain fetal myofiber growth. Gene expression analysis of $dy^{W-/-}$ E17.5 muscles identified a significant increase in the expression of the JAK-STAT target gene *Pim1* and muscles from 2-day and 3-week old $dy^{W-/-}$ mice demonstrate a dramatic increase in pSTAT3 relative to WT muscles. Interestingly, myotubes lacking integrin $\alpha7\beta1$, a laminin-receptor, also show a significant increase in pSTAT3 levels compared with WT myotubes, indicating that $\alpha7\beta1$ can act as a negative regulator of STAT3 activity. Our data reveal for the first time that $dy^{W-/-}$ mice exhibit a myogenesis defect already *in utero*. We propose that overactivation of JAK-STAT signaling is part of the mechanism underlying disease onset and progression in $dy^{W-/-}$ mice.

[†]These authors contributed equally to this work.

Received: August 8, 2016. **Revised:** January 30, 2017. **Accepted:** March 2, 2017

Introduction

Merosin-deficient congenital muscular dystrophy (CMD) type 1A (MDC1A), or laminin-α2 CMD (LAMA2-CMD), is a devastating neuromuscular disease in which patients demonstrate hypotonia from birth. Human MDC1A was initially described by Tomé *et al.* and is caused by mutations in the *LAMA2* gene (1–3), which encodes the laminin α2 chain of laminins 211 and 221 (4). Laminin 211 is the predominant laminin isoform in the basement membrane surrounding adult muscle fibers, while laminin 221 localizes specifically to neuromuscular junctions (5,6). Laminin 211 is crucial for myofiber survival (7,8), and is involved in the regulation of the autophagy-lysosome pathway and the ubiquitin-proteasome system (9,10).

It is generally believed that the absence of laminin 211 around myofibers in MDC1A patients causes a constant stress on these cells, which progressively damages them, inducing muscle wasting, inflammation and fibrosis (11). Since infants are already affected at birth, the muscle weakness underlying the disease must already have arisen during development *in utero*. However, it is unclear when and how disease begins in MDC1A.

Mouse skeletal muscle development starts at E8.5 when Pax3- and/or Pax7-positive muscle stem cells at the edges of the dermomyotome are induced to initiate the myogenic program and differentiate into myotomal myocytes (12–14). The myogenic program involves the expression of one or more of the myogenic regulatory factors (MRFs), the transcription factors Myf5, MyoD, Mrf4 and myogenin (15). From E11.5 until E14.5, these myocytes fuse with differentiating primary myoblasts giving rise to primary (embryonic) myofibers of the trunk muscles, while dermomyotome-derived Pax3-positive cells have migrated and differentiate into the primary myofibers of limbs, tongue and diaphragm (16–20). Subsequently, from E14.5 until birth, Pax7-positive muscle stem cells within the muscle masses undergo a second wave of differentiation into secondary myoblasts. These myoblasts then use the primary myofibers as a scaffold and fuse with each other, generating secondary (fetal) myofibers, and subsequently fuse with both primary and secondary myofibers, increasing their size (17,20). Thus fetal skeletal muscle grows both by addition of new myofibers (hyperplasia) and by fusion of myoblasts to existing myofibers, increasing their size (cell-mediated hypertrophy).

Laminins 111 and 511 are thought to play a role in early stages of myogenesis in the somites (21) and laminins 211, 411 and 511 are found in fetal muscles (5). However, little is known about the exact assembly dynamics and specific roles of the different laminin isoforms during myogenesis. It has been suggested that α4- and α5-laminins can compensate for the absence of α2-laminins during myogenesis *in utero* (5,22), but this hypothesis has not been formally tested.

Here, we perform a detailed analysis of the assembly dynamics of the different laminin isoforms during normal mouse skeletal muscle development. We then use the dy^{W} mouse model for MDC1A to study the effect of laminin α2-chain deficiency on skeletal muscle development *in vivo*. We demonstrate that myotomal and primary myogenesis proceed without defects in $dy^{W-/-}$ embryos. However, during secondary myogenesis, $dy^{W-/-}$ muscles exhibit impaired growth, fail to maintain the normal number of Pax7-positive muscle stem cells and experience a dramatic drop in the number of myogenin-positive myoblasts. This $dy^{W-/-}$ muscle defect correlates with an overactivation of JAK-STAT signaling as well as a dysregulation of Myostatin signaling which we suggest hampers the amplification of the pool of mononucleated muscle cells necessary for cell-mediated hypertrophy of myofibers. We show for the first time that MDC1A starts before birth in $dy^{W-/-}$ mice and that the onset of the disease *in utero* is marked by impaired fetal myogenesis.

Results

Myotomal and primary myogenesis proceed normally in $dy^{W-/-}$ embryos

Our first aim was to detect the stage of MDC1A onset during mouse development. We first characterized myotome development in E10.5 $dy^{W-/-}$ embryos. Immunostaining (for *n* numbers; see Supplementary Material, Tables S1 and S2) with a pan-muscle laminin antibody demonstrates that the laminin matrices lining the dermomyotome and the myotome are normal in $dy^{W-/-}$ embryos (Fig. 1A, A′, C and C′). The mouse *Lama2* gene is normally expressed by myotomal myocytes (Fig. 2D and F) and laminin α2 chain localizes to the myotomal basement membrane in a similar pattern to laminin α1 and α5 chains (Fig. 2A, B, E′ and G′). Laminin α1 and α2 chains are also detected in a patchy pattern among myotomal myocytes (Fig. 2A, E, E′, G and G′) and this pattern is unperturbed in $dy^{W-/-}$ embryos (Fig. 1A, A′, C and C′). Together these observations suggest that the distribution of laminin 111 and 511 is normal in $dy^{W-/-}$ embryos.

Immunostaining for myosin heavy chain (MHC) on sections of E10.5 $dy^{W-/-}$ embryos and their WT littermates shows that myotome morphology and size in $dy^{W-/-}$ embryos is not significantly different from that of WT embryos (Fig. 1A, A″, C, C″ and M; $n = 4$ per genotype). Immunolabeling for Pax3, Pax7 and myogenin did not reveal any differences between WT and $dy^{W-/-}$ embryos (Fig. 1E–G and I–K). TUNEL analysis showed no increase in apoptosis in $dy^{W-/-}$ myotomes (Fig. 1B and D) and phospho-histone 3 (pH3) labeling was similar in WT compared with $dy^{W-/-}$ embryos (Fig. 1H and L). We therefore conclude that myotomal myogenesis proceeds normally in E10.5 $dy^{W-/-}$ embryos.

To analyze if primary myogenesis proceeds normally after E10.5 in $dy^{W-/-}$ embryos, we quantified the total number of primary myofibers in three epaxial deep back muscles (see Materials and Methods) of E17.5 $dy^{W-/-}$ fetuses and their WT littermates, stained with an antibody to slow myosin. This quantification shows that WT and $dy^{W-/-}$ embryos form the same number of primary myofibers (Fig. 1N; $n = 3–6$ per genotype). In fact, our analysis of laminin deposition during primary myogenesis (E11.5–E13.5) in normal embryos supports this hypothesis. Immunostaining with pan-muscle laminin antibody (Fig. 2H and H′) (23,24) and with antibodies for α2 (Fig. 2I), α1 and α5 chains (data not shown) failed to detect a laminin-containing basement membrane around primary myotubes. These results indicate that primary myogenesis is normally laminin independent (see Fig. 3P).

These data show that myotome development and primary myogenesis are not significantly affected in $dy^{W-/-}$ embryos.

Laminins 411 and 511 line myofibers and Pax7-positive cells in fetal $dy^{W-/-}$ muscles

We next determined the normal dynamics of laminin assembly during fetal muscle development by immunohistochemistry. Laminin assembly around myofibers starts at E14.5 (Fig. 3A), i.e. precisely at the beginning of secondary myogenesis (17). In agreement with, and expanding on the data by Patton *et al.* (5), we find that laminin assembly around myofibers involves

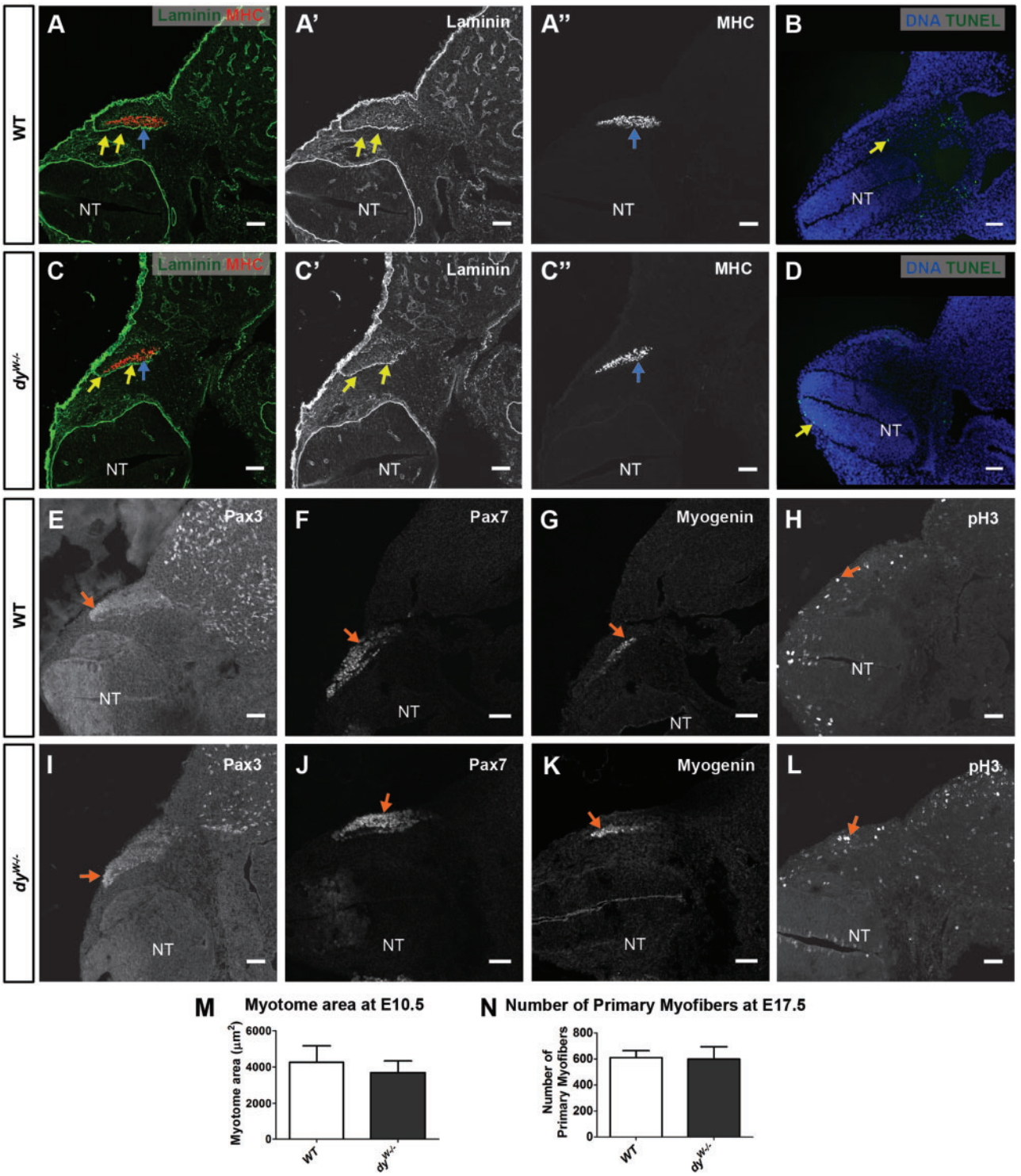

Figure 1. Normal myotomal and primary myogenesis in $dy^{W-/-}$ embryos. Transverse sections of E10.5 WT (**A** and **B**, **E–H**) and $dy^{W-/-}$ embryos (**C** and **D**, **I–L**). (A–A″ and C–C″) Immunohistochemistry for pan-muscle laminin (yellow arrows) and MHC (blue arrows) in WT and $dy^{W-/-}$ embryos. (B and D) Apoptosis (TUNEL assay) in WT and $dy^{W-/-}$ embryos (yellow arrows in B and D). (E–G and I–K) Immunostaining for Pax3 (E and I), Pax7 (F and J) and myogenin (G and K) in WT (arrows in E–G) and $dy^{W-/-}$ (arrows in I–K) embryos. (H and L) pH3 immunostaining (arrows) in WT (H) and $dy^{W-/-}$ (L) embryos. (**M**) Quantification of myotome cross sectional area in E10.5 WT and $dy^{W-/-}$ embryos. (**N**) Quantification of slow-myosin positive myofibers in E17.5 WT and $dy^{W-/-}$ epaxial muscles. Data in M and N are represented as mean ± SEM. See Supplementary Material, Table S2 for *n* numbers. NT, neural tube. Dorsal is on the left. Scale bars: 50 μm.

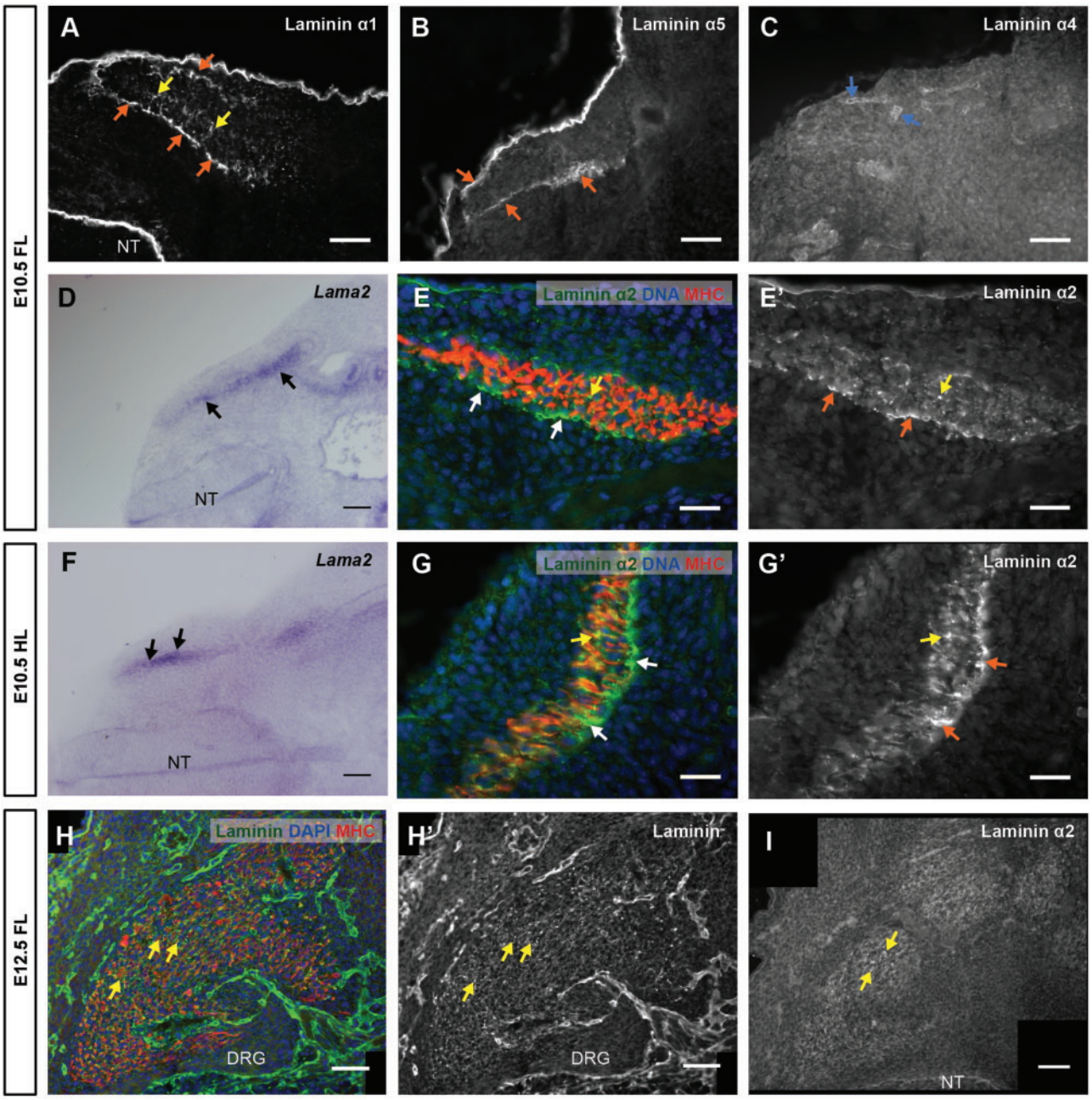

Figure 2. First phase of laminin assembly during mouse myogenesis: the myotome. (**A–G′**) Transverse sections of CD-1 E10.5 embryos at forelimb (A–E′) and hindlimb (F–G′) levels stained by immunofluorescence (A–C, E, E′, G and G′) or by *in situ hybridization* (D and F). (A–C) Immunostaining for laminin α1 (A), α5 (B) and α4 (C) chains. (D and F) *In situ* hybridization for *Lama2*. (E, E′, G and G′) Immunostaining for α2 laminin and MHC with DNA (DAPI) staining (E and G) and grayscale image of α2 laminin immunostaining (E′ and G′). (**H** and **I**) Transverse sections of CD-1 E12.5 embryos at forelimb level stained by immunofluorescence. (H and H′) Immunostaining for laminin (pan-muscle laminin antibody) and MHC, with DNA staining (H), and grayscale image of immunostaining with pan-muscle laminin antibody (H′). (**I**) Immunofluorescence for laminin α2 chain. See Supplementary Material, Table S1 for *n* numbers. FL, Forelimb; HL, Hindlimb; NT, neural tube; DRG, dorsal root ganglia; MHC, myosin heavy chain. Dorsal is on the left, except (G) and (G′) where dorsal is down. Scale bars: 50 μm (A–D,F,H–I); 25 μm (E,E′,G,G′).

laminins containing the α2, α4 and α5 chains (Fig. 3B–D), while laminin α1 is absent (data not shown; see Fig. 4C). The myofiber basement membrane is discontinuous at E14.5 (Fig. 3A–D), but then grows progressively in subsequent stages (E15.5: Fig. 3E–H and M; E17.5: Fig. 3I–L). Pax7-positive muscle stem cells are reported to enter their niche under the myofiber basement membrane at around E16.5 (25,26). Consistent with this notion, we observed a progressive increase in laminin coverage near Pax7-positive cells between E15.5 (Fig. 3N, N′ and N″) and E17.5 (Fig. 3O, O′ and O″). Thus during normal fetal myogenesis, laminins 211, 411 and 511 are gradually assembled around myofibers (see Fig. 3P) and by E17.5 most Pax7-positive muscle stem cells reside underneath the myofiber basement membrane.

It has previously been suggested that laminin α4 and α5 chains may play a role in compensating for the absence of α2 chain laminins during development (5,22). Indeed, at E17.5 these two laminin chains are detected around both WT and $dy^{W-/-}$ myofibers (Fig. 4A, B, E and F). The laminin α1 chain,

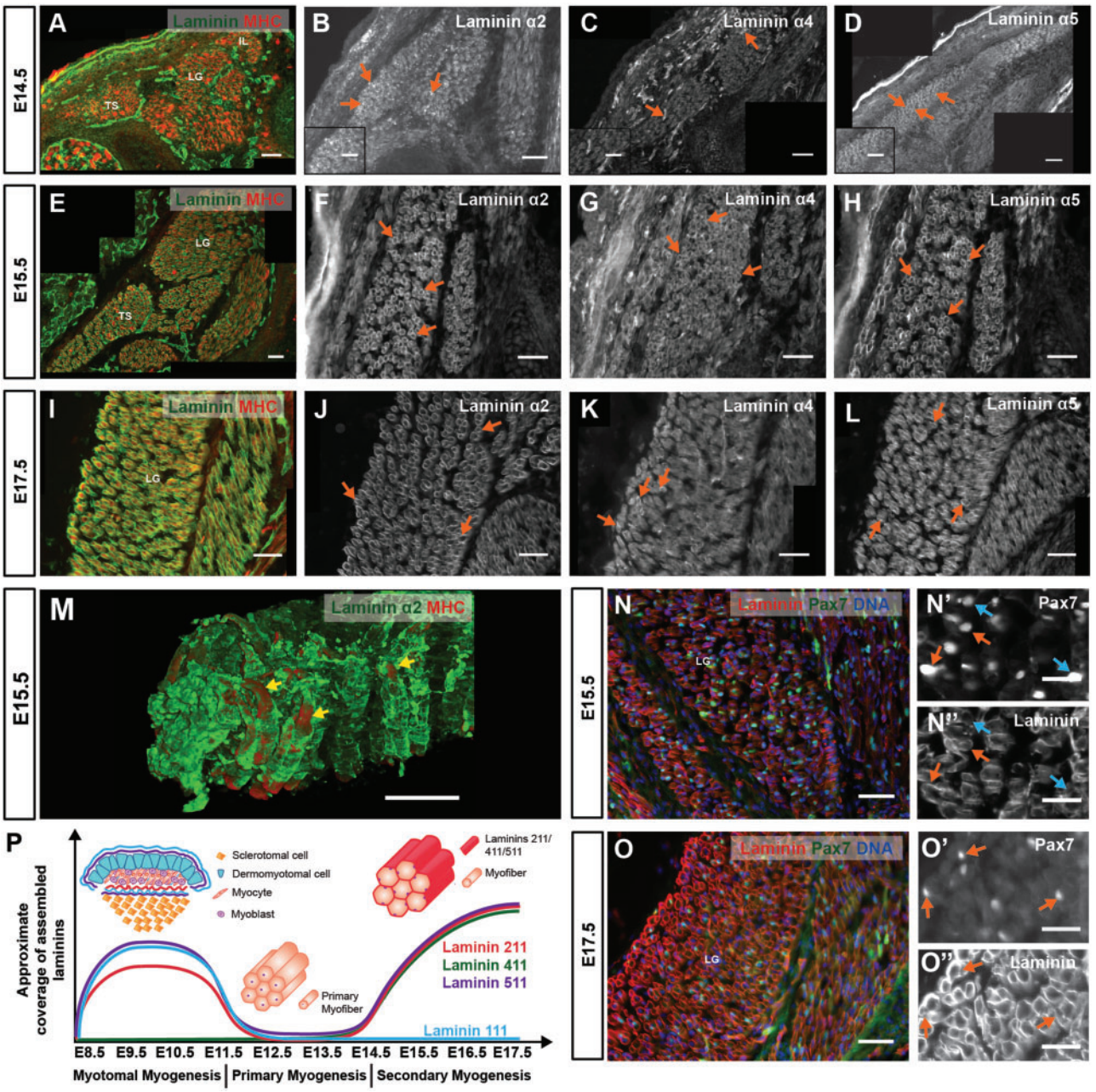

Figure 3. Second phase of laminin assembly during mouse myogenesis: secondary myogenesis. (**A–L**) Transverse sections of CD-1 E14.5 (A–D), E15.5 (E–H) and E17.5 (I–L) fetuses at forelimb level showing epaxial muscles stained by immunohistochemistry for pan-muscle laminin (A, E and I), laminin α2 (B, F and J), α4 (C, G and K) and α5 (D, H and L) chains. (**M**) 3D reconstruction of whole mount E15.5 epaxial muscles showing double immunohistochemistry for laminin α2 and MHC. (**N–O″**) Immunohistochemistry on transverse sections of E15.5 (N and N″) and E17.5 (O and O″) epaxial muscles with pan-muscle laminin and Pax7 antibodies with DNA (DAPI) staining. (**P**) Schematic representation of laminin assembly dynamics over time during myotomal, primary and secondary myogenesis. See Supplementary Material, Table S1 for *n* numbers. TS, transversospinalis; LG, longissimus; IL, iliocostalis; MHC, myosin heavy chain. Dorsal is on the left. Scale bars: 50 μm (A–O); 25 μm (N′, N″, O′ and O″).

normally absent in WT muscles, is not upregulated in fetal $dy^{W-/-}$ muscles (Fig. 4C and G). Thus, in terms of laminin α-chain immunoreactivity, fetal WT and $dy^{W-/-}$ muscles only differ in that the α2 chain is absent in the $dy^{W-/-}$ (see inserts in Fig. 4C and G), as previously reported for adult $dy^{W-/-}$ muscles (27,28). The localization of the α7 subunit of the α7β1 integrin (Fig. 4D and H) and the α-subunit of dystroglycan (Fig. 4I and J), both laminin receptors, is also not affected in $dy^{W-/-}$ when compared with WT fetuses. Double immunostaining for Pax7 and laminins shows that Pax7-positive cells are in close contact with laminin α4 and α5 chains in both WT and $dy^{W-/-}$ muscles (Fig. 4K–N″). Moreover, Pax7-positive cells in $dy^{W-/-}$ muscles at PN2 remain covered by laminins (Fig. 4O, O′ and O″). We conclude that fetal $dy^{W-/-}$ muscles contain laminins 411 and 511 as well as the α7β1 integrin and dystroglycan in a pattern very similar to the one observed in the WT.

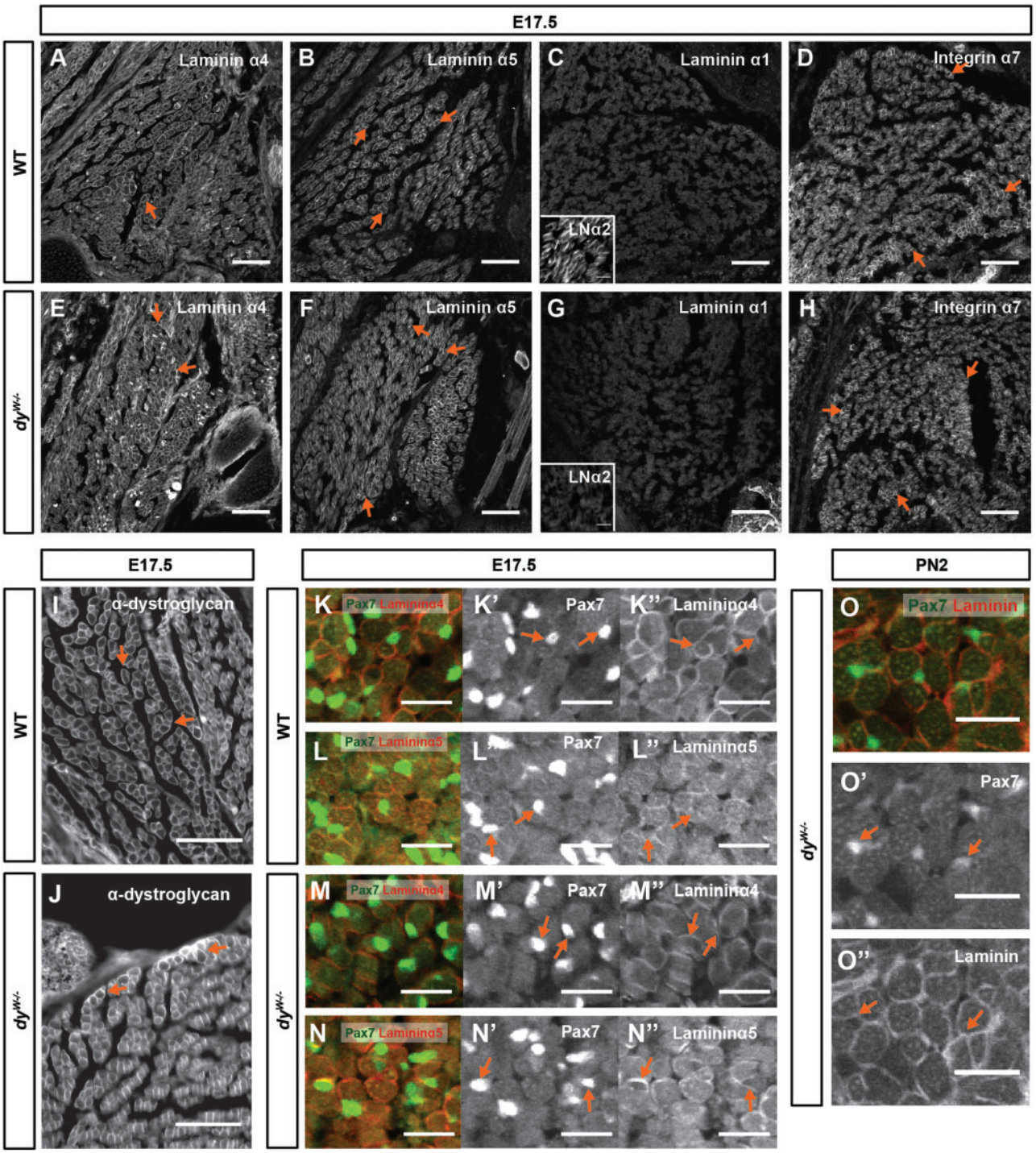

Figure 4. Laminins 411 and 511 line integrin α7β1- and α-dystroglycan-positive myofibers and Pax7-positive cells in $dy^{W-/-}$ muscles. (**A–J**) Immunostaining for laminin α4 (A and E), α5 (B and F), α1 (C and G), α2 (inserts in C and G) chains, integrin α7 subunit (D and H) and α-dystroglycan (I and J) in epaxial muscles of E17.5 WT (A–D and I) and $dy^{W-/-}$ (E–H and J) fetuses. (**K–N″**) Double immunostaining for Pax7 and laminin α4 (K, K″, M and M″) and laminin α5 (M, M″, N, and N″) on transverse sections of epaxial muscles of E17.5 WT (K–N″) and $dy^{W-/-}$ (M–N″) fetuses. (**O–O″**) Double immunostaining for Pax7 and pan-muscle laminin on transverse sections of PN2 $dy^{W-/-}$ epaxial muscles. $n \geq 3$ fetuses/pups per genotype/stage and staining, except for α7 integrin ($n=2$ per genotype) and laminin α2 ($n=1$ per genotype). LNα2, laminin α2. Dorsal is to the left and medial is up. Scale bars: 100 μm (A–J); 50 μm (K–O″).

$dy^{W-/-}$ fetuses display impaired muscle growth

We next asked whether laminins 411 and 511 are able to compensate for the lack of functional laminin 211 during fetal and early postnatal stages of development. To this end we compared the development of $dy^{W-/-}$ muscles with that of WT muscles at E15.5–E18.5 and PN2 (Fig. 5; Supplementary Material, Fig. S1). Overall muscle morphology, as viewed by MHC and pan-muscle laminin immunostaining, appears to be normal in $dy^{W-/-}$ when compared with WT fetuses and PN2 pups (Supplementary

Material, Fig. S1A–J). High-magnification images of pan-muscle laminin staining demonstrate that, despite the absence of laminin 211 in $dy^{W-/-}$ fetuses (insert in Fig. 4G) the pattern of total laminin in WT and $dy^{W-/-}$ fetuses and PN2 pups is indistinguishable (Fig. 5A–J). Measurements of the area of three epaxial muscle groups (transversospinalis, longissimus and iliocostalis; see Materials and Methods) revealed that fetal WT and $dy^{W-/-}$ muscles do not differ in size at E15.5 and E16.5, but that from E17.5 onwards $dy^{W-/-}$ muscles are smaller than WT muscles (Fig. 5K). This difference is significant for E18.5 where $dy^{W-/-}$ muscles have a mean area of 497 170 ± 26 028 μm^2 compared with 607 274 ± 26 626 μm^2 for WT muscles (Fig. 5K; $P = 0.023$; $n = 4$–5 per genotype) and remains significant for PN2 where $dy^{W-/-}$ muscles have a mean area of 707 547 ± 52 802 μm^2 compared with 975 901 ± 56 748 μm^2 for WT muscles (Fig. 5K; $P = 0.021$, $n = 3$–4 per genotype). In spite of this difference in muscle area, the number of myofibers present in WT and $dy^{W-/-}$ fetuses at E15.5–E18.5 does not differ (Fig. 5L) and, although $dy^{W-/-}$ have on average slightly fewer myofibers at PN2, this difference did not reach statistical significance (Fig. 5L; $P = 0.088$; $n = 3$–4 per genotype).

We conclude that although $dy^{W-/-}$ fetuses generate a normal number of myofibers during fetal development, $dy^{W-/-}$ muscles fail to grow normally, being significantly smaller than WT muscles from E18.5 onwards. These results suggest that laminin 211 is essential for the normal growth of fetal muscles and that laminin 411 and 511 are unable to compensate for its absence.

Fetal $dy^{W-/-}$ muscles fail to fully expand their pool of Pax7-positive muscle stem cells and generate fewer differentiated myoblasts

To address the cellular mechanism behind the impaired muscle growth in $dy^{W-/-}$ fetuses, we used immunohistochemistry for Pax7 and myogenin in sections of WT and $dy^{W-/-}$ fetuses and PN2 pups to detect muscle stem cells and differentiated myoblasts, respectively. During normal WT fetal myogenesis, there is a steady increase in the number of Pax7-positive cells in the muscle masses between E15.5 and E17.5 (Fig. 5M; gray line), and the number of Pax7-positive cells stays stable between E17.5 and E18.5 (Fig. 5M; gray line). This occurs even though this pool of cells also feeds into the myogenin-positive pool through differentiation (Fig. 5N; gray line). Quantification of the number of Pax7- and myogenin-positive cells shows that these are at first normal in $dy^{W-/-}$ muscles (Fig. 5M and N; black lines), but between E17.5 and E18.5 there is a dramatic reduction in the number of both Pax7- and myogenin-positive cells in $dy^{W-/-}$ (Fig. 5M and N; black lines) compared with WT muscles (Fig. 5M and N; gray lines). E18.5 $dy^{W-/-}$ fetuses have a mean number of 348 ± 52 Pax7-positive cells per section and thus display a 31% reduction in the number of these cells compared with WT fetuses which have a mean number of 502 ± 39 cells, this difference being statistically significant (Fig. 5M; $P = 0.047$; $n = 5$ per genotype). Thus, whereas E18.5 WT muscles have on average 0.19 Pax7-positive cells/myofiber per section, $dy^{W-/-}$ muscles have 0.13 Pax7-positive cells/myofiber (Supplementary Material, Table S3). E18.5 $dy^{W-/-}$ fetuses show a 47% reduction in the number of myogenin-positive cells compared with WT fetuses, as $dy^{W-/-}$ muscles have an average of 113 ± 12 myogenin-positive cells per section and WT muscles have an average of 212 ± 21 cells and this difference is statistically significant (Fig. 5N; $P = 0.008$; $n = 4$ per genotype). E18.5 WT muscles therefore have an average of 0.08 myogenin-positive cells/myofiber per section, while $dy^{W-/-}$ muscles have only 0.04 myogenin-positive cells/myofiber (Supplementary Material, Table S3). This reduction in the number of Pax7- and myogenin-positive cells in $dy^{W-/-}$ muscles is not due to cell death (Fig. 5O–R), nor to a significant reduction in the number of cells undergoing mitosis (Fig. 5S; $P = 0.515$; $n = 4$–5 per genotype).

In normal WT muscles, the number of Pax7- and myogenin-positive cells goes down between E18.5 and PN2 (Fig. 5M and N; gray lines). Our quantitative data show that the number of Pax7-positive cells in the muscles of $dy^{W-/-}$ PN2 pups is similar to WT pups at PN2 (Fig. 5M; $P = 0.394$; $n = 4$ per genotype), suggesting that the number of Pax7-positive cells diminishes precociously in $dy^{W-/-}$ relative to WT muscles. Furthermore, the number of myogenin-positive cells, although more variable among individuals of both genotypes, is also very similar in $dy^{W-/-}$ relative to WT muscles at PN2 (Fig. 5N; $P = 0.528$; $n = 3$ per genotype). To validate our cell count data at PN2, we isolated PN2 epaxial muscles and assessed Pax7 and myogenin protein levels. Interestingly, Pax7 and myogenin protein levels in $dy^{W-/-}$ PN2 muscles are increased 1.5- and 1.6-fold, respectively, compared with WT pups (Fig. 5T).

Together these data demonstrate that $dy^{W-/-}$ fetal muscles undergo a precocious drop in the number of Pax7- and myogenin-positive cells, which correlates with the significant reduction in cross-sectional area observed in E18.5 $dy^{W-/-}$ muscles. At PN2 the numbers of Pax7- and myogenin-positive cells are similar in WT and $dy^{W-/-}$ muscles and Pax7 and myogenin protein levels are actually increased in $dy^{W-/-}$ relative to WT muscles. However, regardless of this apparent recovery, the difference in cross-sectional area between WT and $dy^{W-/-}$ muscles does not diminish; rather it becomes larger indicating that increased Pax7 and myogenin protein levels does not translate into an actual recovery (Fig. 5K).

$dy^{W-/-}$ muscles display an overactivation of the JAK-STAT signaling pathway

We next applied an RT-qPCR approach to assess for potential changes in the following signaling pathways known to be modulators of muscle growth: Wnt/β-catenin (29,30), Notch (31–34), JAK-STAT (35–37) and Myostatin (GDF8) (38–41). These experiments were done on muscles isolated from E17.5 fetuses, i.e. immediately before $dy^{W-/-}$ muscles are significantly different from WT muscles in terms of a cross-sectional area and the number of Pax7- and myogenin-positive cells.

We did not detect significant differences in transcript levels of the Wnt signaling target genes *Axin2* and *Wisp1* in $dy^{W-/-}$ when compared with WT fetal muscles (Fig. 6A). Transcript levels of the Notch target genes *Dll1*, *HeyL* and *Hey1* were also not different between $dy^{W-/-}$ and WT muscles (Fig. 6B). However, transcripts for the JAK-STAT signaling target gene *Pim1* were significantly increased (Fig. 6C; a 42% increase; $P = 0.007$) in $dy^{W-/-}$ muscles, while *Bcl6* and *Myc* were unchanged (Fig. 6C). Finally, the Myostatin signaling target gene *Akirin1*, which is negatively regulated by Myostatin (42), was significantly increased in $dy^{W-/-}$ compared with WT muscles (Fig. 6D; a 27% increase; $P = 0.027$). *Cdkn1a*, which encodes for p21 and can be regulated by Myostatin signaling (40), demonstrates a slight, but not significant, increase in transcript levels in $dy^{W-/-}$ fetuses (Fig. 6D). Together, these results point to the possibility that an overactivation of the JAK-STAT signaling pathway and a down-regulation of the Myostatin signaling pathway in E17.5 $dy^{W-/-}$ muscles may underlie the myogenesis defect identified at E18.5.

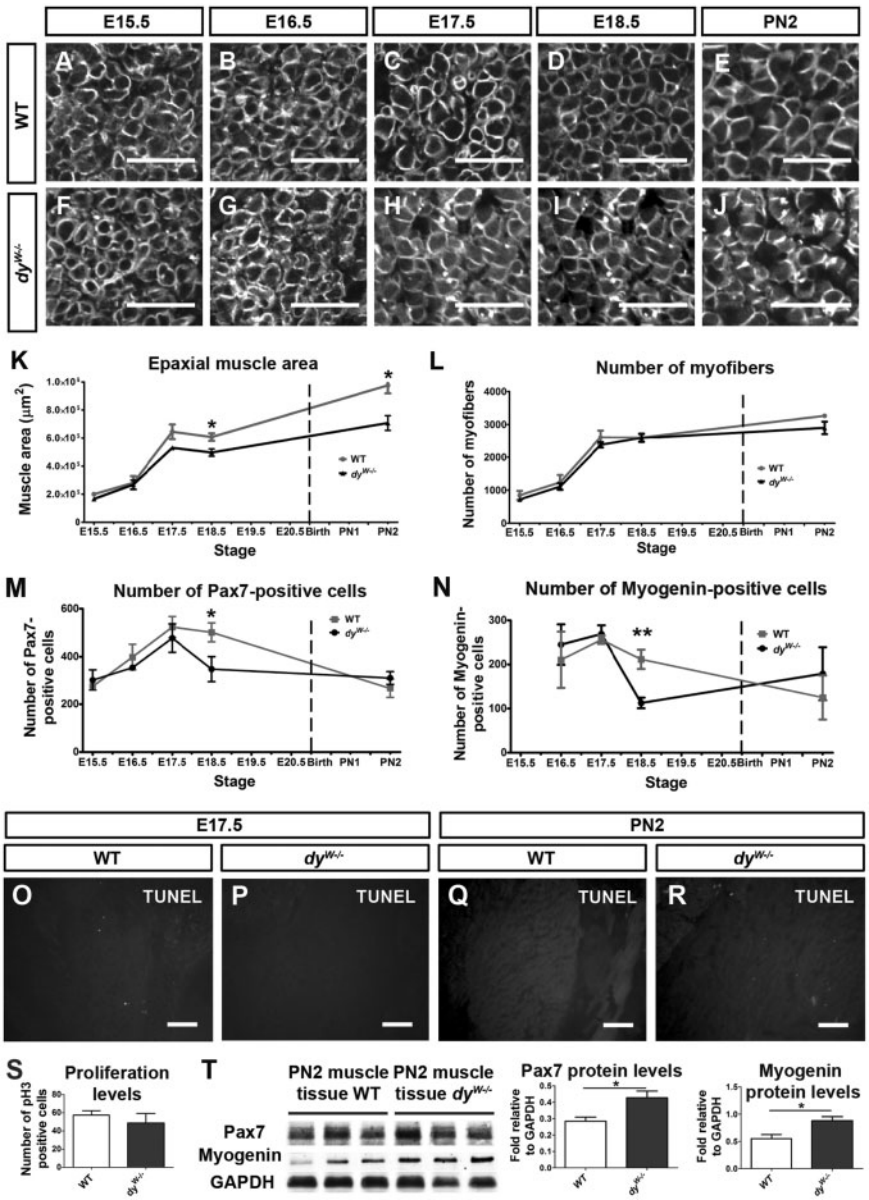

Figure 5. $dy^{W-/-}$ fetuses display a myogenesis defect. (**A–J**) High magnification images of pan-muscle laminin immunostaining on transverse sections of WT (A–E) and $dy^{W-/-}$ (F–J) epaxial muscles at E15.5 (A and F), E16.5 (B and G), E17.5 (C and H), E18.5 (D and I) and PN2 (E and J) showing that fiber shape and laminin coverage is unaffected in $dy^{W-/-}$ compared with WT muscles. (**K**) Graph showing cross sectional area of epaxial WT (gray line) and $dy^{W-/-}$ (black line) muscles from E15.5 to E18.5 and PN2. (**L**) Graph showing myofiber number in the same epaxial muscles from E15.5 to E18.5 and PN2. (**M** and **N**) Graphs showing the quantification of Pax7- (M) and myogenin-positive (N) cells in fetal and PN2 WT (gray lines) and $dy^{W-/-}$ (black lines) epaxial muscles . (**O–R**) TUNEL assay on transverse section of WT (O and Q) and $dy^{W-/-}$ (P and R) muscles at E17.5 (O and P) and PN2 (Q and R). (**S**) Graph showing the number of pH3-positive cells in E17.5 WT and $dy^{W-/-}$ muscles. (**T**) Western blot quantification of Pax7 and myogenin proteins in PN2 WT and $dy^{W-/-}$ muscles. See Supplementary Material, Figure S1 for images of entire composite sections of epaxial muscle groups and Supplementary Material, Table S2 for *n* numbers for (A–S). Data in (K–N), (S and T) is represented as mean ± SEM (*$P < 0.05$; **$P < 0.01$). Scale bars: 50 μm (A–J); 100 μm (O–R).

To test this hypothesis further, we quantified the amount of phosphorylated STAT3 (Tyr 705) (pSTAT3) in E17.5 back muscles using SureFire analysis. This assay revealed that $dy^{W-/-}$ back muscles have, on average, more pSTAT3 compared with control muscles, but this difference was not statistically significant (Fig. 6E; $P = 0.131$; $n = 4$–6 per genotype group). We then isolated protein from the back muscles of PN2 pups and performed Western blot analysis for pSTAT3 (Tyr 705). The results revealed a 3.4-fold and statistically significant ($P = 0.002$) increase in pSTAT3 levels in $dy^{W-/-}$ compared with WT muscles (Fig. 6F). Furthermore, pSTAT3 levels remain significantly higher in 3-week old $dy^{W-/-}$ compared with WT muscles (Fig. 6H; $P = 0.012$). Together, these data demonstrate that $dy^{W-/-}$ muscles display a significant increase in JAK-STAT signaling from very early on, possibly as early as E17.5, and that pSTAT3 activity remains significantly higher in the muscles of 3-week old $dy^{W-/-}$ mice.

Inflammatory cells and fibrotic tissues are known to secrete cytokines that may augment JAK-STAT signaling (43). However, fetal and PN2 $dy^{W-/-}$ muscles were morphologically normal at all stages studied (Fig. 5A–J; Supplementary Material, Fig. S1A–J)

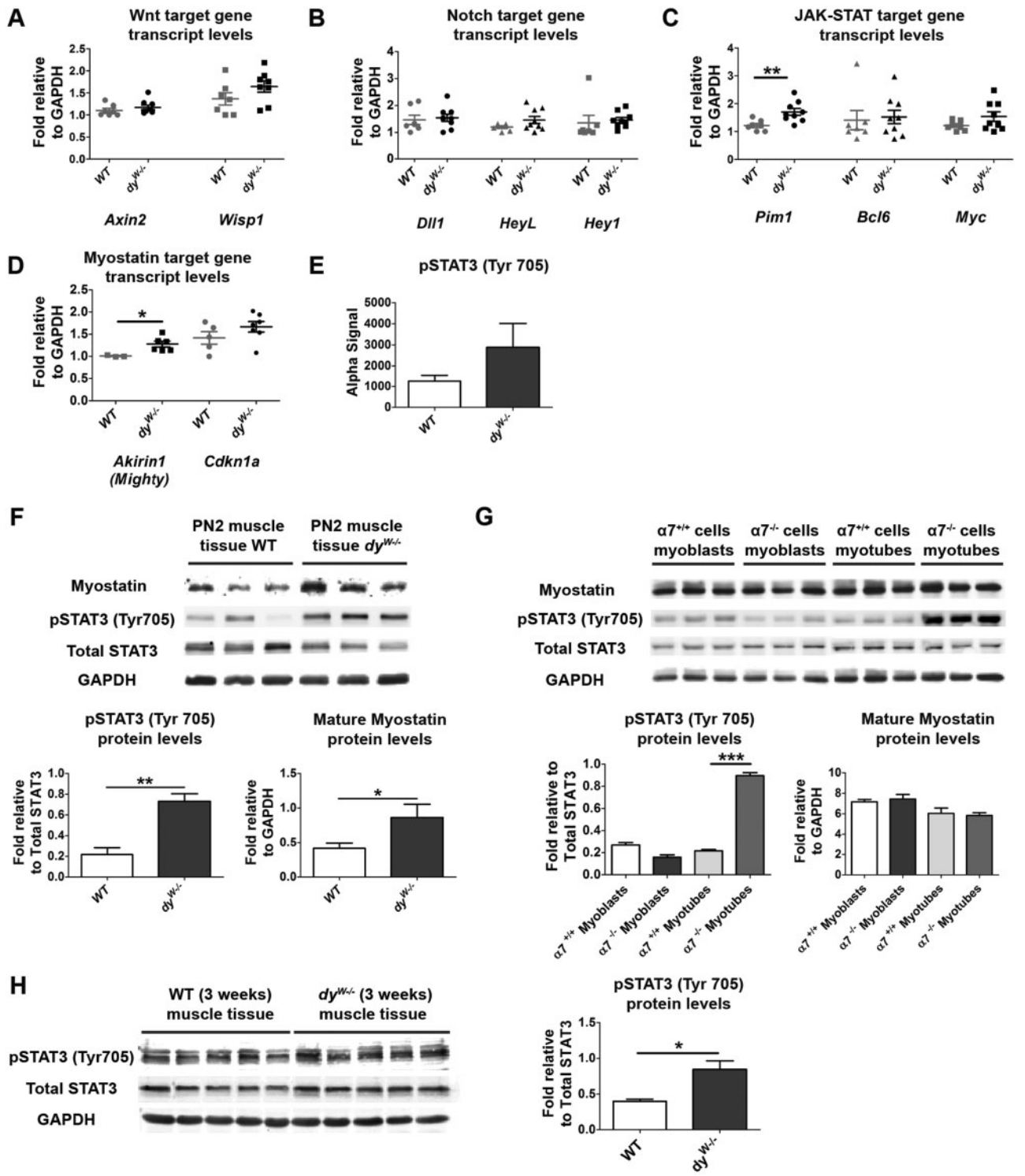

Figure 6. Assessment of the mechanism underlying disease onset in $dy^{W-/-}$ muscles. (**A–D**) RT-qPCR analysis of the expression of Wnt, Notch, JAK-STAT and Myostatin signaling pathway members and target genes in E17.5 WT and $dy^{W-/-}$ epaxial muscles. (**E**) SureFire analysis of pSTAT3 (Tyr 705) signal in E17.5 control versus $dy^{W-/-}$ muscles. (**F**) Western blot analysis of pSTAT3 (Tyr 705) and mature Myostatin in WT and $dy^{W-/-}$ PN2 muscles. (**G**) Western blot analysis of pSTAT3 and mature Myostatin in cultured $\alpha7^{+/+}$ and $\alpha7^{-/-}$ myoblasts and myotubes. (**H**) Western blot analysis of pSTAT3 levels in triceps muscle of 3-week old WT and $dy^{W-/-}$ mice. Data represented as mean ± SEM (*P <0.05; **P <0.01; ***P <0.001).

and did not display any infiltration of macrophages at E17.5 or PN2 (as assessed by CD11b immunolabeling; data not shown) nor any increase in Sirius Red staining at PN2 (data not shown). Thus, these results exclude inflammation and fibrosis as the reason for the increased pSTAT3 activity detected in E17.5 and PN2 $dy^{W-/-}$ muscles.

Interestingly, mature Myostatin protein levels were also significantly increased (2.1-fold; $P = 0.049$) in PN2 $dy^{W-/-}$ muscles

when compared with WT (Fig. 6F) indicating that, unlike at E17.5 where our RT-qPCR results indicate a reduction in Myostatin signaling, at PN2 mature Myostatin protein is upregulated in $dy^{W-/-}$ muscles.

Laminin 211 is known to bind to and signal through the α7β1 integrin receptor (44,45). To assess whether the α7β1 integrin modulates the JAK-STAT and/or Myostatin signaling pathways, we measured pSTAT3 and mature Myostatin levels in $\alpha7^{-/-}$ and control $\alpha7^{+/+}$ myoblasts and myotubes. No significant differences were detected between $\alpha7^{-/-}$ and $\alpha7^{+/+}$ myoblasts (Fig. 6G). Mature Myostatin levels were also not significantly different in $\alpha7^{-/-}$ compared with $\alpha7^{+/+}$ myotubes (Fig. 6G). However, pSTAT3 levels were dramatically increased (3.1-fold; $P < 0.0001$) in $\alpha7^{-/-}$ myotubes compared with $\alpha7^{+/+}$ myotubes (Fig. 6G). These results demonstrate that whereas the α7β1 integrin does not appear to affect JAK-STAT signaling in myoblasts, it is a potent negative regulator of JAK-STAT signaling in myotubes.

Together, these results implicate increased pSTAT3 activity in early stages of $dy^{W-/-}$ pathology through a mechanism that seems to involve the α7β1 integrin on myotubes. Moreover, we also provide evidence for a dysregulation of Myostatin signaling in $dy^{W-/-}$ compared with WT muscles as Myostatin signaling is reduced in $dy^{W-/-}$ fetal muscles masses but then mature Myostatin levels are increased in these muscles after birth.

Discussion

MDC1A starts during development *in utero* in the $dy^{W-/-}$ mouse model

Here we reveal for the first time that MDC1A in the $dy^{W-/-}$ mouse starts during development *in utero*. Although laminins containing the α2-chain are first detected during myotome development, this phase of myogenesis proceeds normally in $dy^{W-/-}$ embryos. Laminin 111 and 511 are present during myotome development (this study, 5,21) and we find that both laminin α1 and laminin α2 are detected within the E10.5 myotome, suggesting laminin 111 is able to compensate for the absence of laminin 211 in the myotome. Consistent with this hypothesis, overexpression of a laminin α1 transgene (46) and laminin 111 protein therapy ameliorate pathology in laminin α2-deficient mice (47,48).

Strikingly, primary myogenesis appears to proceed in the total absence of assembled laminins both in trunk and limbs (this study, 23) suggesting that this phase of myogenesis is laminin-independent. Accordingly, we verified that primary myogenesis proceeds normally in $dy^{W-/-}$ embryos.

Laminin assembly around myotubes resumes at E14.5, at the very beginning of secondary (fetal) myogenesis, with the assembly of laminins 211, 411 and 511, but not laminin 111 (this study, 5). We find that these laminins progressively come to line myofibers and Pax7-positive muscle stem cells as they enter their niche at around E16.5 (25,26,49). Fetal myogenesis is characterized by intense muscle growth, which occurs in two ways: (1) by the generation of secondary myofibers (hyperplasia) most of which occurs until E18.0 (26) and (2) through growth of these secondary myofibers, as well as the preexisting primary myofibers, through fusion of myoblasts to these fibers (cell-mediated hypertrophy) (17,20). Our data show that WT and $dy^{W-/-}$ fetuses display similar myofiber numbers. However, our data indicate that between E17.5 and E18.5, $dy^{W-/-}$ fetuses exhibit an impairment in cell-mediated hypertrophy, which is not rescued by the presence of laminins 411 and 511. Our measurements show that the area of $dy^{W-/-}$ muscles is 82% of that of WT muscles at E18.5 and is 75% of WT muscles at PN2, indicating that muscle growth starts lagging behind at E18.5 and that the effect is more pronounced at PN2. Reduced myofiber cross sectional area is indeed one of the hallmarks of disease in $dy^{W-/-}$ animals as the cross-sectional area of triceps brachii myofibers in 5-week old $dy^{W-/-}$ animals is, on average, ∼50% that of same stage WT muscle (47). Moreover, intramuscular injections of laminin 111 into tibialis anterior muscle of 3-week old $dy^{W-/-}$ animals increases the cross sectional area of this muscle by 65% compared with that of PBS injected control $dy^{W-/-}$ animals (48). Together, these observations demonstrate that the presence of laminin 211 (or the closely related laminin 111) acts positively on muscle growth. Here we demonstrate that $dy^{W-/-}$ muscle growth starts lagging behind already *in utero*, before any signs of muscle pathology are detected, which leads us to propose that the onset of MDC1A disease in $dy^{W-/-}$ mice involves a defect in cell-mediated hypertrophy during fetal myogenesis.

Overactivation of JAK-STAT marks $dy^{W-/-}$ disease onset

Our results suggest that the STAT3 signaling pathway is overactivated in $dy^{W-/-}$ muscles and that the link between laminin 211 and STAT3 signaling lies in the α7β1 integrin, since integrin α7-null myotubes *in vitro* show a dramatic upregulation of pSTAT3 compared with control myotubes. It has already been extensively demonstrated that integrin α7β1 signaling plays an important role in disease progression of *Lama2*-deficient mice (7,49,50). Curiously, α7-null myoblasts do not show any increase in pSTAT3. However, myoblasts *in vitro* do not fully represent the diversity of mononucleated muscle cell *in vivo*. Indeed, previous studies have shown that JAK-STAT3 overactivation in satellite cells promotes aging and impairs their expansion during muscle repair (36,37). Thus we cannot exclude the possibility that $dy^{W-/-}$ fetuses display an increased STAT3 phosphorylation in a subset of mononucleated muscle cells. Altogether, these results indicate that a major function of laminin 211 in myofibers is to attenuate STAT3 signaling via the α7β1 integrin.

E18.5 $dy^{W-/-}$ fetal muscles have 31% fewer Pax7-positive cells than WT muscles which demonstrates that these muscles are unable to maintain normal levels of self-renewal of muscle stem cells. We see no indication of cell death, nor differences in pH3-positive cell numbers, excluding increased apoptosis or impaired proliferation as the reason for the drop in Pax7-positive cells. Muscle stem cell amplification is achieved by symmetric divisions of Pax7-positive cells which originate two Pax7-positive stem cells, whereas asymmetric divisions maintain one Pax7-positive stem cell while simultaneously generating a committed cell which later differentiates and fuses with the muscle fiber (51–53). The 3D organization of the myofiber basement membrane favors symmetric divisions of Pax7-positive cells (54). Furthermore, an intact laminin matrix in the Pax7-positive stem cell niche is essential for their self-renewal (55). Thus laminin 211-deficiency is likely to alter the nature of the satellite cell niche as well as its 3D organization. Interestingly, satellite cells cultured on isolated myofibers under conditions that inhibit JAK-STAT signaling show a significant increase in the frequency of symmetric cell divisions and a decrease in asymmetric divisions (36). Thus we suggest a model where altered laminin composition and/or overactivation of JAK-STAT signaling in fetal $dy^{W-/-}$ muscles increases the frequency of asymmetric cell divisions at the expense of symmetric cell divisions, thus leading to a precocious reduction in the

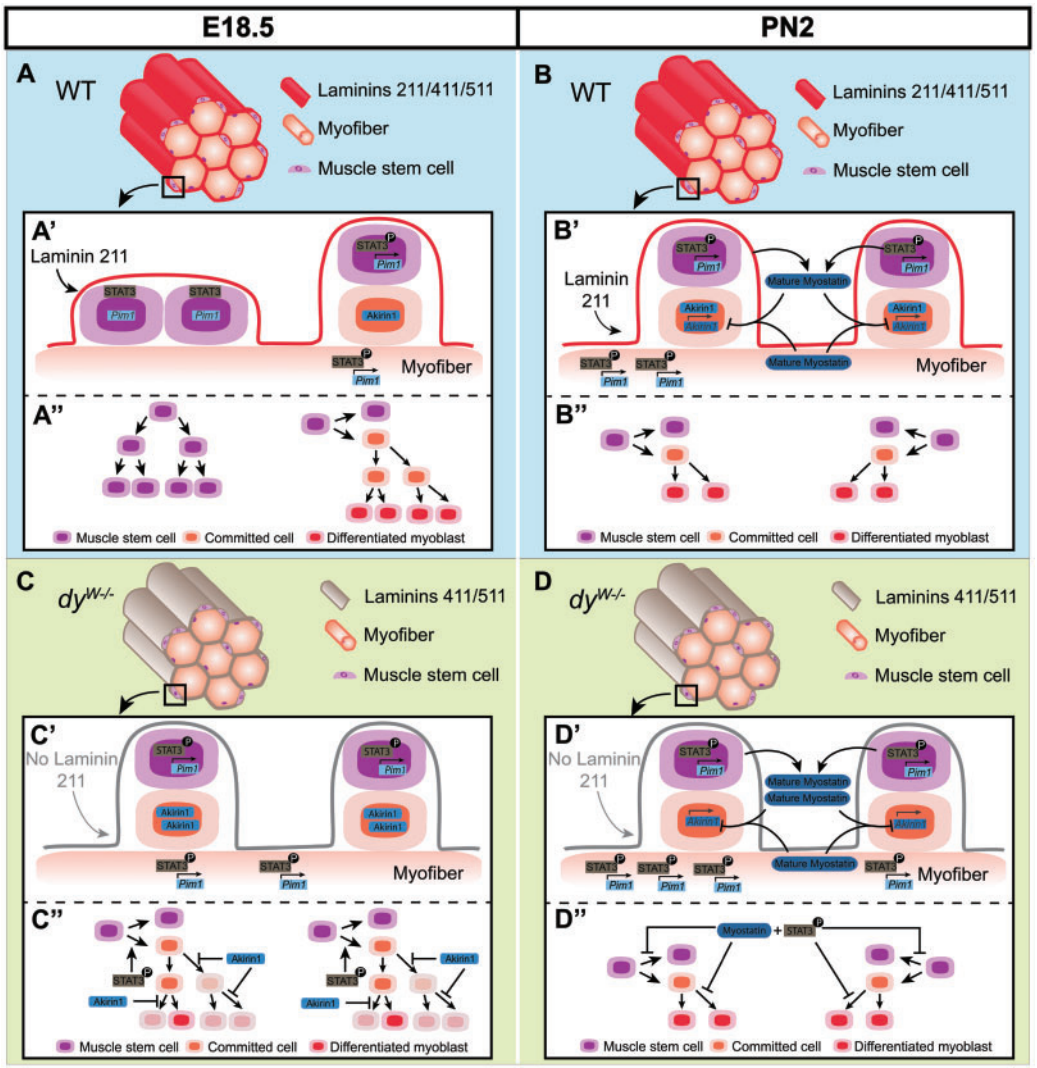

Figure 7. Model illustrating possible mechanism of disease onset during $dy^{W-/-}$ fetal muscle development. Illustration of muscles in normal (WT; **A** and **B**) and *Lama2*-deficient ($dy^{W-/-}$; **C** and **D**) mice at fetal E18.5 (A and C) and postnatal PN2 (B and D) stages. A close-up of the surface of a muscle fiber shows two muscle stem cell division events (A′–D′) and the proposed results of these divisions (A″–D″) in WT (A′, A″, B′ and B″) and $dy^{W-/-}$ (C′, C″, D′ and D″) muscles at E18.5 (A′, A″, C′ and C″) and PN2 (B′, B″, D′ and D″). *Lama2*-deficiency results in a significant reduction in the number of Pax7- and myogenin-positive cells at E18.5 compared with same stage WT muscles. This may occur due to an increase in the frequency of asymmetric cell divisions at the expense of amplifying symmetric divisions (A′ and C′), either because of altered laminin composition (absence of laminin 211) and/or an increase in pSTAT3 activity (A′ and C′). Consequently, E18.5 $dy^{W-/-}$ muscles would have fewer Pax7-positive muscle stem cells than WT muscles (A″ and C″). We further propose that, due to an increased expression of *Aikirin1* (A′ and C′), committed cells in fetal $dy^{W-/-}$ muscles would display impaired expansion capacity, leading to fewer terminally differentiated myoblasts (A″ and C″; shaded cells in C″ would not be generated). Therefore, E18.5 $dy^{W-/-}$ muscles have fewer myogenin-positive, terminally differentiated myoblasts than WT muscles (A″ and C″). In normal postnatal muscle, the frequency of asymmetric cell divisions increases and expansion of muscle stem cells and committed cells decreases. This is illustrated by showing only asymmetric cell divisions in WT (B′ and B″) and $dy^{W-/-}$ muscles (D′ and D″) and fewer cell divisions of committed cells in both WT (B″) and $dy^{W-/-}$ muscles (D″). *Lama2*-deficiency continues to lead to increased levels of pSTAT3 post-natally and in addition leads to the concomitant increase in mature myostatin levels (B′ and D′). Although PN2 $dy^{W-/-}$ muscles are significantly smaller than WT muscles they have similar numbers of stem cells and differentiated cells at this stage (B″ and D″). Thus the rate of asymmetric divisions appears to be similar in WT and $dy^{W-/-}$ PN2 muscles. However, the joint overactivation of JAK-STAT and Myostatin signaling at PN2 could exert a progressive impairment on the division capacity of muscle stem cells and committed cells in $dy^{W-/-}$ individuals (B″ and D″) with consequences for subsequent stages. This effect may later have a negative impact on the regeneration capacity of $dy^{W-/-}$ muscles.

number of Pax7-positive cells in $dy^{W-/-}$ relative to WT muscles (Fig. 7A and C).

Our results also show that E18.5 $dy^{W-/-}$ fetal muscles have an even more dramatic reduction in myogenin-positive cells. This suggests that E18.5 $dy^{W-/-}$ fetal muscles also experience an impaired generation of normal numbers of differentiated and fusion-competent myoblasts. However, increased JAK-STAT signaling leads to an increase in MyoD levels (35–37,56). A possible explanation may lie in the concomitant and significant upregulation of *Akirin1* (*Mighty*) in $dy^{W-/-}$ muscles at E17.5. *Akirin 1* is negatively regulated by Myostatin signaling and is known to activate MyoD in satellite cells (40,42,57). Normally, committed myoblasts can undergo one or two cell divisions before MyoD activates p21, inducing cell cycle exit (58). Interestingly, $Mstn^{-/-}$ fetuses exhibit a drop in the number of Pax7- and myogenin-positive cells at E18.5, which the authors suggest is due to an overactivation of MyoD in committed cells, leading to their faster exit from the cell cycle and formation of

fewer differentiated and fusion-competent cells (41). We thus suggest that the drop in myogenin-positive cells observed in E18.5 $dy^{W-/-}$ muscles may be due to an attenuation of Myostatin signaling which makes committed cells differentiate faster and without significant amplification (Fig. 7A and C).

Taken together we propose a model for MDC1A onset (Fig. 7A and C) where the absence of laminin 211 around fetal myofibers and/or an overactivation of JAK-STAT signaling shift the balance of muscle stem cell divisions to asymmetric divisions, leading to a reduction in the renewal rate of the Pax7-positive muscle stem cell pool. Furthermore, the simultaneous attenuation in Myostatin signaling inhibits the normal amplification of committed cells, leading to a drop in the number of myogenin-positive cells, formation of fewer fusion-competent myoblasts and, consequently, an impairment in fiber growth.

$dy^{W-/-}$ pups start life with significantly smaller muscles and do not possess the machinery to recover their size

In agreement with the situation in human MDC1A patients who have smaller muscles at birth (3), we found that $dy^{W-/-}$ pups are born with significantly smaller muscles than WT pups. Although $dy^{W-/-}$ pups no longer differ from WT pups in the number of Pax7- and myogenin-positive cells, $dy^{W-/-}$ pups have not recovered from the impaired growth during fetal myogenesis. In fact, the apparent recovery of Pax7-positive cell numbers in $dy^{W-/-}$ pups is not due to an increase in Pax7-positive cells in $dy^{W-/-}$ muscles. Rather it is due to a decrease in the number of Pax7-positive cells in WT muscles between E18.5 and PN2. Indeed, a gradual drop in Pax7-positive cell numbers is known to occur during normal postnatal development with the progressive increase in the frequency of asymmetric cell divisions (59). Moreover, muscle stem cells experience a change in identity between fetal and postnatal stages of development, where their capacity for self-renewal goes down while the potency to either differentiate or to recolonize the satellite cell niche increases (60). Our data show that fetal $dy^{W-/-}$ muscles experience a premature decrease in the number of Pax7-positive cells suggesting that they make the transition to a postnatal identity too early.

PN2 pups show a significant increase in pSTAT3 activity (Fig. 7B and D), suggesting that continuous laminin 211-integrin α7β1 signaling is normally required to dampen this signaling pathway. Curiously, in contrast to the situation observed at E17.5 where Myostatin signaling appears to be attenuated, $dy^{W-/-}$ PN2 muscles display higher levels of mature Myostatin compared with WT muscles (Fig. 7B and D). The reason for this is unclear, but a simultaneous increase in pSTAT3 and Myostatin is characteristic of aged muscle, and is thought to be a major factor in the observed loss of regeneration potential during muscle aging (61,62). Consistent with this notion, the muscles of $dy^{W-/-}$ mice have a dramatic reduction in regeneration capacity (48,63).

We therefore propose that $dy^{W-/-}$ muscles display an aged phenotype where, at each time-point from fetal development to adulthood, the muscle environmental cues resemble that of substantially older muscles.

Conclusions

In the present study, we provide the first evidence of *in utero* defects in a mouse model for MDC1A. This marks a paradigm shift in our understanding of MDC1A disease pathogenesis because rather than putting deteriorating muscle fiber health as a first step in the disease, our data demonstrate that the primary defect in $dy^{W-/-}$ mice arises because of impaired in fetal myogenesis. Our results also uncovered the relevance of JAK-STAT and Myostatin pathways in $dy^{W-/-}$ disease onset and progression, which emphasizes the importance of these pathways as targets for future therapies. Taken together, our study provides an important framework for future *in utero* therapies and highlights the necessity for prenatal disease diagnosis and early intervention.

Materials and Methods

Mice and genotyping

dy^{W} mice (gift from Eva Engvall via Paul Martin; The Ohio State University, Columbus, OH, USA) have a *LacZ-neo* cassette inserted in the *Lama2* gene, and homozygous animals produce a small amount of a truncated laminin α2 protein lacking the N-terminal LN domain (27,28). Heterozygous dy^{W} mice were crossed to obtain homozygous $dy^{W-/-}$ mutants and wild-type (WT) controls. Fetuses heterozygous for the dy^{W} allele were indistinguishable from WT controls in all parameters measured (data not shown) and were thus used as controls together with WT fetuses in the SureFire assay. Outbred Charles River CD-1 mice (Envigo, Spain) were used to assess the distribution of laminin variants during normal myogenesis (Figs 2 and 3).

The day of the vaginal plug was designated embryonic day (E) 0.5 and embryos were staged as in Kaufman (64). Anesthetized pregnant females were sacrificed by cervical dislocation, uterine horns removed and placed in cold phosphate buffered saline (PBS) with Ca^{2+} and Mg^{2+} where embryos (E10.5–E13.5) and fetuses (E14.5–E18.5) were dissected out. Post-natal day 2 (PN2) pups were anesthetized by hypothermia and sacrificed by decapitation. Embryos for *in situ* hybridization were collected in PBS.

Embryos, fetuses and pups from heterozygous dy^{W} crossings were genotyped with the following primers: 5′ ACTGCCCTTTC TCACCCACCCTT 3′, 5′ GTTGATGCGCTTGGGACTG 3′ and 5′ GTC GACGACGACAGTACTGGCCTCAG 3′.

All procedures involving mice were performed under two approved protocols: (3/2016) from the Animal Welfare Body of the Faculty of Sciences, University of Lisbon and (000404) from the Institutional Animal Care and Use Committee of the University of Nevada.

Cell culture

Myoblasts isolated previously from gastrocnemius muscles of 10-day old $\alpha7\beta gal^{+/+}$ and $\alpha7\beta gal^{-/-}$ mice (65) were cultured in six-well plates until confluence in Dulbecco's modified Eagle medium (DMEM) (GIBCO) supplemented with 20% fetal bovine serum (Atlanta Biologicals), 0.5% chick-embryo extract (Seralab), 2 mM L-glutamine (GIBCO) and penicillin/streptomycin (100 U/ml; GIBCO) at 37°C with 5% CO_2. Myotubes were obtained by differentiating $\alpha7\beta gal^{+/+}$ and $\alpha7\beta gal^{-/-}$ myoblasts during 5 days in DMEM supplemented with 1% horse serum (Atlanta Biologicals), 2mM L-glutamine (GIBCO) and penicillin/streptomycin (100 U/ml; GIBCO).

In situ hybridization

To determine the mRNA expression pattern of *Lama2* (66), E10.5 embryos were fixed in 4% paraformaldehyde (PFA) in PBS for

whole mount *in situ* hybridization as described previously (66). Briefly, embryos were hybridized overnight at 70°C and probe localization was detected with alkaline phosphatase-conjugated anti-dioxygenin antibodies and NBT/BCIP (Roche) as a substrate. The number of embryos used is listed in Supplementary Material, Table S1.

Immunohistochemistry

Embryos were fixed in 0.2% PFA in 0.12M phosphate buffer (PB) overnight at 4°C. Fetuses and PN2 pups were fixed in 2% PFA in PB for 2 days at 4°C. Embryos, fetuses and PN2 pups were cryo-embedding and 12 μm cryosections were processed for immunohistochemistry essentially as in Bajanca *et al.* (67). However, cryosections of fetuses and PN2 pups were incubated with 0.2% Triton X-100 in PBS for 20 min at room temperature before blocking with 5% bovine albumin serum in PBS. Antigen retrieval was done in E15.5-PN2 tissue by immersing sections in Tris–EDTA (10 mM Tris base, 1 mM EDTA, 0.05% Tween 20) buffer, pH 9.0 at 95°C for 20 min. When staining with monoclonal mouse antibodies, the Mouse-On-Mouse (MOM) kit (Vector Laboratories) was used.

Antibodies used are listed in Supplementary Material, Table S4. The polyclonal antibody against EHS-laminin (i.e. laminin 111) (4) detects all laminins containing α1, β1 or γ1 chains (68). Since all laminin isoforms in skeletal muscle contain at least the γ1 chain, we used this polyclonal anti-laminin antibody to detect all muscle laminins and designate it pan-muscle laminin antibody. TUNEL assay was performed using DeadEnd Fluorometric TUNEL System (Promega). DNA was visualized with 4,6-diamidino-2-phenylindole (DAPI, 5 μg/ml, Sigma). The number of embryos, fetuses and PN2 pups processed for immunohistochemistry and/or TUNEL assay are listed in Supplementary Material, Tables S1 and S2.

Whole mount immunohistochemistry

Whole mount immunohistochemistry was performed as described previously (69). Briefly, dissected fetal back muscles were incubated with primary and secondary antibodies for 2 days at 4°C and were washed for a full day after each antibody incubation. For nuclear staining fetal muscles were incubated with Topro3 (T3605; Molecular Probes; 1:400) and 10 mg/ml ribonuclease A (55674; Calbiochem; 1:100) together with the secondary antibodies. Antibodies used are listed in Supplementary Material, Table S4.

SureFire

AlphaLISA SureFire Ultra kit for p-STAT3 (Tyr705) (ALSU-PST3-A500) was performed according to the manufacturer's instructions (Perkin Elmer). Ten micrograms of protein extract were used per sample for this assay.

Western blotting

Protein extracts were collected in radioimmunoprecipitation assay buffer (RIPA) with 5 mM NaF, 10 mM Na_3VO_4 and a protease inhibitor cocktail (Thermo Scientific; 1:500) and stored at −80°C. After quantification using Pierce BCA protein assay kit (Thermo Scientific), protein extracts were separated with SDS 10 or 12% polyacrylamide gel electrophoresis and transferred to nitrocellulose membranes. Signals were detected using WesternSure™ PREMIUM Chemiluminescent Substract (LICOR) and detection with an Odyssey imaging system (Li-Cor Biosciences). Normalization was performed with glyceraldehyde 3-phosphate dehydrogenase (GAPDH) and/or total STAT3. Quantifications were performed in Fiji (http://fiji.sc/Fiji). Western blots on myoblasts and myotubes were done in triplicate. Muscle tissue from at least 5 PN2 and 3-week old mice per genotype were used. Antibodies used are listed in Supplementary Material, Table S4.

Real time quantitative RT-PCR

RNA was extracted from E17.5 back muscles with Trizol Reagent kit (Ambion, Life Technologies). First-strand cDNA synthesis was performed using the SuperScript III First-Strand Synthesis System for RT-PCR kit (Ambion, Life Technologies). Real-Time qPCR reactions were performed in triplicates with 2× PowerUp SYBR Green Master Mix (Life Technologies) and 500 ng RNA. Transcript levels were normalized against *Gapdh* expession and the fold change was calculated using ΔΔCt method. Primers used are listed in Supplementary Material, Table S5.

Image analysis and quantifications

Sections processed for *in situ* hybridization were photographed using an Olympus DP50 camera coupled to an Olympus BX51 microscope. Sections processed for immunohistochemistry were either imaged with a Hamamatsu Orca R2 camera coupled to an Olympus BX60 fluorescence microscope, or images were acquired on an Olympus IX81 or Leica SPE confocal microscope system. The acquired images were analyzed in Fiji version 1.49 and imported to Amira V.5.3.3 (Visage Imaging, Inc.) software as described previously (69,70).

Transverse sections processed for immunohistochemistry were used for muscle cross-sectional area measurements and quantification of total myofibers, primary myofibers, Pax7- and myogenin-positive cells. To ensure maximum standardization, quantifications were always done in three specific epaxial muscle groups (transversospinalis, longissimus and iliocostalis) at forelimb level and three to five sections per staining and embryo/fetus/PN2 pup were used. Overlapping confocal images covering the three specific epaxial muscles were obtained with a 20× lens and individual images were then stitched together into a large composite image (see Supplementary Material, Fig. S1) using the Fiji plugin Pairwise Stitching (71). Areas were measured using a drawing tool to line the muscles in Fiji and quantifications were performed using Fiji plugin Cell Counter (http://fiji.sc/Cell_Counter). We consider the sum of the number of Pax7- and myogenin-positive cells as a close estimate for the total number mononucleated muscle cells in the muscle masses (Supplementary Material, Table S3) (20). All measurements and counts were done in a blinded fashion.

Statistical analysis

Student's *t*-test was used to test for differences between mRNA, protein or pSTAT3 levels in muscle samples from WT and $dy^{W-/-}$ fetuses and/or PN2 pups, and $\alpha7^{+/+}$ and $\alpha7^{-/-}$ cells, considering $P < 0.05$ as statistically significant. Student's *t*-test was also used to test for differences in the number of Pax7- and myogenin-positive cells in sections of WT and $dy^{W-/-}$ muscles. Finally, differences in muscle cross-sectional area and myofiber numbers were tested using a nested ANOVA where individuals

were nested within genotypes (WT or $dy^{W-/-}$). As described above, all parameters were quantified in stitched composite images of three to five sections per individual, each section covering the same three muscle groups. Each stage was tested separately. Statistical analyses were performed using GraphPad Prism 5 and STATISTICA 12 software.

Supplementary Material

Supplementary Material is available at *HMG* online.

Acknowledgements

We thank Jeff Miner for generously sharing his anti-α5 and anti-α4 laminin antibodies, Madeleine Durbeej for kindly giving the anti-α1 antibody and Patrícia Ybot-Gonzalez for the *Lama2* probe. The MF20, Pax3, Pax7 and IIH6 C4 antibodies were developed by D.A. Fischman, C.P. Ordahl, A. Kawakami and K.P. Campbell, respectively, and were obtained from the Developmental Studies Hybridoma Bank, developed under the auspices of the NICHD and maintained by The University of Iowa, Department of Biology, Iowa City, IA 52242, USA. We also thank Inês Fragata, Jorge Palmeirim and Margarida Bárbaro for help with the statistical analysis, Inês Antunes for help in the laboratory, Patrícia Gomes de Almeida for help with image processing and for critically reviewing the manuscript and all members of our groups for suggestions and constant support.

Conflict of Interest statement. None declared.

Funding

This work was supported by Fundação para a Ciência e a Tecnologia (FCT, Portugal) (project PTDC/SAU-BID/120130/2010, SFRH/BD/86985/2012 scholarship to A.M.N and SFRH/BPD/65370/2009 scholarship to M.D.), Association Française contre les Myopathies (AFM) Téléthon (contract n° 19959), CureCMD, Struggle Against Muscular Dystrophy (SAM), NIH/NIAMS (R01AR064338-01A1), the University of Nevada, Reno (USA) and Mick Hitchcock Scholarship (to A.S. and T.F.).

References

1. Helbling-Leclerc, A., Zhang, X., Topaloglu, H., Cruaud, C., Tesson, F., Weissenbach, J., Tomé, F.M., Schwartz, K., Fardeau, M., Tryggvason, K., *et al.* (1995) Mutations in the laminin α2-chain gene (*LAMA2*) cause merosin-deficient congenital muscular dystrophy. *Nat. Genet.*, **11**, 216–218.
2. Naom, I.S., D'Alessandro, M., Topaloglu, H., Sewry, C., Ferlini, A., Helbling-Leclerc, A., Guicheney, P., Weissenbach, J., Schwartz, K., Bushby, K., *et al.* (1997) Refinement of the laminin α2 chain locus to human chromosome 6q2 in severe and mild merosin deficient congenital muscular dystrophy. *J. Med. Genet.*, **34**, 99–104.
3. Tomé, F.M., Evangelista, T., Leclerc, A., Sunada, Y., Manole, E., Estournet, B., Barois, A., Campbell, K.P. and Fardeau, M. (1994) Congenital muscular dystrophy with merosin deficiency. *C.R. Acad. Sci. III*, **317**, 351–357.
4. Aumailley, M., Bruckner-Tuderman, L., Carter, W.G., Deutzmann, R., Edgar, D., Ekblom, P., Engel, J., Engvall, E., Hohenester, E., Jones, J.C.R., *et al.* (2005) A simplified laminin nomenclature. *Matrix Biol.*, **24**, 326–332.
5. Patton, B.L., Miner, J.H., Chiu, A.Y. and Sanes, J.R. (1997) Distribution and function of laminins in the neuromuscular system of developing, adult, and mutant mice. *J. Cell Biol.*, **139**, 1507–1521.
6. Patton, B.L. (2000) Laminins of the neuromuscular system. *Microsc. Res. Tech.*, **51**, 247–261.
7. Vachon, P.H., Xu, H., Liu, L., Loechel, F., Hayashi, Y., Arahata, K., Reed, J.C., Wewer, U.M. and Engvall, E. (1997) Integrins (α7β1) in muscle function and survival. Disrupted expression in merosin-deficient congenital muscular dystrophy. *J. Clin. Invest.*, **100**, 1870–1881.
8. Laprise, P., Vallé, K., Demers, M.J., Bouchard, V., Poirier, E.M., Vézina, A., Reed, J.C., Rivard, N. and Vachon, P.H. (2003) Merosin (laminin-2/4)-driven survival signalling: complex modulations of Bcl-2 homologs. *J. Cell. Biochem.*, **89**, 1115–1125.
9. Carmignac, V., Svensson, M., Körner, Z., Elowsson, L., Matsumura, C., Gawlik, K.I., Allamand, V. and Durbeej, M. (2011a) Autophagy is increased in laminin α2 chain-deficient muscle and its inhibition improves muscle morphology in a mouse model of MDC1A. *Hum. Mol. Genet.*, **20**, 4891–4902.
10. Carmignac, V., Quéré, R. and Durbeej, M. (2011b) Proteasome inhibition improves the muscle of laminin α2 chain-deficient mice. *Hum. Mol. Genet.*, **20**, 541–552.
11. Gawlik, K.I. and Durbeej, M. (2011) Skeletal muscle laminin and MDC1A: pathogenesis and treatment strategies. *Skelet. Muscle*, **1**, 1–13.
12. Venters, S., Thorsteinsdóttir, S. and Duxson, M.J. (1999) Early development of the myotome in the mouse. *Dev. Dyn.*, **216**, 219–232.
13. Gros, J., Scaal, M. and Marcelle, C. (2004) A two-step mechanism for myotome formation in chick. *Dev. Cell*, **6**, 875–882.
14. Hollway, G. and Currie, P. (2005) Vertebrate myotome development. *Birth Defects Res. C Embryo Today*, **75**, 172–179.
15. Buckingham, M. (2006) Myogenic progenitor cells and skeletal myogenesis in vertebrates. *Curr. Opin. Genet. Dev.*, **16**, 525–532.
16. Cinnamon, Y., Kahane, N. and Kalcheim, C. (1999) Characterization of the early development of specific hypaxial muscles from the ventrolateral myotome. *Development*, **126**, 4305–4315.
17. Biressi, S., Molinaro, M. and Cossu, G. (2007) Cellular heterogeneity during vertebrate skeletal muscle development. *Dev. Biol.*, **308**, 281–293.
18. Deries, M., Schweitzer, R. and Duxson, M.J. (2010) Developmental fate of the mammalian myotome. *Dev. Dyn.*, **239**, 2898–2910.
19. Thorsteinsdóttir, S., Deries, M., Cachaço, A.S. and Bajanca, F. (2011) The extracellular matrix dimension of skeletal muscle development. *Dev. Biol.*, **354**, 191–207.
20. Tajbakhsh, S. (2009) Skeletal muscle stem cells in developmental versus regenerative myogenesis. *J. Intern. Med.*, **266**, 372–389.
21. Bajanca, F., Luz, M., Raymond, K., Martins, G.G., Sonnenberg, A., Tajbakhsh, S., Buckingham, M. and Thorsteinsdóttir, S. (2006) Integrin α6β1-laminin interactions regulate early myotome formation in the mouse embryo. *Development*, **133**, 1635–1644.
22. Ringelmann, B., Ro, C., Hallmann, R., Maley, M., Davies, M., Grounds, M. and Sorokin, L. (1999) Expression of laminin α1, α2, α4, and α5 chains, fibronectin, and tenascin-C in skeletal muscle of dystrophic 129ReJ *dy/dy* mice. *Exp. Cell Res.*, **246**, 165–182.
23. Cachaço, A.S., Pereira, C.S., Pardal, R.G., Bajanca, F. and Thorsteinsdóttir, S. (2005) Integrin repertoire on myogenic

cells changes during the course of primary myogenesis in the mouse. *Dev. Dyn.*, **232**, 1068–1078.
24. Deries, M., Gonçalves, A.B., Vaz, R., Martins, G.G., Rodrigues, G. and Thorsteinsdóttir, S. (2012) Extracellular matrix remodelling accompanies axial muscle development and morphogenesis in the mouse. *Dev. Dyn.*, **241**, 350–364.
25. Kassar-Duchossoy, L., Giacone, E., Gayraud-Morel, B., Jory, A., Gomès, D. and Tajbakhsh, S. (2005) Pax3/Pax7 mark a novel population of primitive myogenic cells during development. *Gen. Dev.*, **19**, 1426–1431.
26. Ontell, M. and Kozeka, K. (1984) Organogenesis of the mouse extensor digitorum logus muscle: a quantitative study. *Am. J. Anat.*, **171**, 149–161.
27. Kuang, W., Xu, H., Vachon, P.H., Liu, L., Loechel, F., Wewer, U.M. and Engvall, E. (1998) Merosin-deficient congenital muscular dystrophy. Partial genetic correction in two mouse models. *J. Clin. Invest.*, **102**, 844–852.
28. Guo, L.T., Zhang, X.U., Kuang, W., Xu, H., Liu, L.A., Vilquin, J.-T., Miyagoe-Suzukic, Y., Takeda, S., Ruegg, M.A., Wewer, U.M. and Engvall, E. (2003) Laminin α2 deficiency and muscular dystrophy; genotype-phenotype correlation in mutant mice. *Neuromuscul. Disord.*, **13**, 207–215.
29. Hutcheson, D.A., Zhao, J., Merrell, A., Haldar, M. and Kardon, G. (2009) Embryonic and fetal limb myogenic cells are derived from developmentally distinct progenitors and have different requirements for β-catenin. *Gen. Dev.*, **23**, 997–1013.
30. Le Grand, F., Jones, A.E., Seale, V., Scimè, A. and Rudnicki, M.A. (2009) Wnt7a activates the planar cell polarity pathway to drive the symmetric expansion of satellite stem cells. *Cell Stem Cell*, **4**, 535–547.
31. Mourikis, P., Gopalakrishnan, S., Sambasivan, R. and Tajbakhsh, S. (2012) Cell-autonomous Notch activity maintains the temporal specification potential of skeletal muscle stem cells. *Development*, **139**, 4536–4548.
32. Schuster-Gossler, K., Cordes, R. and Gossler, A. (2007) Premature myogenic differentiation and depletion of progenitor cells cause severe muscle hypotrophy in *Delta1* mutants. *Proc. Natl. Acad. Sci. U.S.A.*, **104**, 537–542.
33. Vasyutina, E., Lenhard, D.C., Wende, H., Erdmann, B., Epstein, J.A., Birchmeier, C. and Delbru, M. (2007) *RBP-J* (*Rbpsuh*) is essential to maintain muscle progenitor cells and to generate satellite cells. *Proc. Natl. Acad. Sci. U.S.A.*, **104**, 4443–4448.
34. Fukada, S., Yamaguchi, M., Kokubo, H., Ogawa, R., Uezumi, A., Yoneda, T., Matev, M.M., Motohashi, N., Ito, T., Zolkiewska, A., *et al.* (2011) Hesr1 and Hesr3 are essential to generate undifferentiated quiescent satellite cells and to maintain satellite cell numbers. *Development*, **138**, 4609–4619.
35. Wang, K., Wang, C., Xiao, F., W.H. and Wu, Z. (2008) JAK2/STAT2/STAT3 are required for myogenic differentiation. *J. Biol. Chem.*, **283**, 34029–34036.
36. Price, F.D., von Maltzahn, J., Bentzinger, C.F., Dumont, N., Yin, H., Chang, N.C., Wilson, D.H., Frenette, J. and Rudnicki, M. (2014) Inhibition of JAK-STAT signalling stimulates adult satellite cell function. *Nat. Med.*, **20**, 1174–1181.
37. Tierney, M.T., Aydogdu, T., Sala, D., Malecova, B., Gatto, S., Puri, P.L., Latella, L. and Sacco, A. (2014) STAT3 signaling controls satellite cell expansion and skeletal muscle repair. *Nat. Med.*, **20**, 1182–1186.
38. McPherron, C., Lawler, M. and Lee, S.J. (1997) Regulation of skeletal muscle mass in mice by a new TGFβ superfamily member. *Nature*, **387**, 83–90.
39. Thomas, M., Langley, B., Berry, C., Sharma, M., Kirk, S., Bass, J. and Kambadur, R. (2000) Myostatin, a negative regulator of muscle growth, functions by inhibiting myoblast proliferation. *J. Biol. Chem.*, **275**, 40235–40243.
40. McCroskery, S., Thomas, M., Maxwell, L., Sharma, M. and Kambadur, R. (2003) Myostatin negatively regulates satellite cell activation and self-renewal. *J. Cell Biol.*, **162**, 1135–1147.
41. Matsakas, A., Otto, A., Elashry, M.I., Brown, S.C. and Patel, K. (2010) Altered primary and secondary myogenesis in the myostatin-null mouse. *Rejuvenation Res.*, **13**, 717–727.
42. Marshall, A., Salerno, M.S., Thomas, M., Davies, T., Berry, C., Dyer, K., Bracegirdle, J., Watson, T., Dziadek, M., Kambadur, R., *et al.* (2008) Mighty is a novel promyogenic factor in skeletal myogenesis. *Exp. Cell Res.*, **314**, 1013–1029.
43. Harrison, D.A. (2012) The JAK/STAT pathway. *Cold Spring Harb. Perspect. Biol.*, **4**, 1–3.
44. Song, W.K., Wang, W., Foster, R.F., Bielser, D.A. and Kaufman, S.J. (1992) H36-α 7 is a novel integrin α chain that is developmentally regulated during skeletal myogenesis. *J. Cell Biol.*, **117**, 643–657.
45. Hodges, B.L., Hayashi, Y.K., Nonaka, I., Wang, W., Arahata, K. and Kaufman, S.J. (1996) Altered expression of the α7β1 integrin in human and murine muscular dystrophies. *J. Cell Sci.*, **110**, 2873–2881.
46. Gawlik, K., Miyagoe-Suzuki, Y., Ekblom, P., Takeda, S. and Durbeej, M. (2004) Laminin α1 chain reduces muscular dystrophy in laminin α2 chain deficient mice. *Hum. Mol. Genet.*, **13**, 1775–1784.
47. Rooney, J.E., Knapp, J.R., Hodges, B.L., Wuebbles, R.D. and Burkin, D.J. (2012) Laminin-111 protein therapy reduces muscle pathology and improves viability of a mouse model of merosin-deficient congenital muscular dystrophy. *Am. J. Pathol.*, **180**, 1593–1602.
48. Van Ry, P.M., Minogue, P., Hodges, B.L. and Burkin, D.J. (2014) Laminin-111 improves muscle repair in a mouse model of merosin-deficient congenital muscular dystrophy. *Hum. Mol. Genet.*, **23**, 383–396.
49. Gawlik, K., Mayer, U., Blomberg, K., Sonnenberg, A., Ekblom, P. and Durbeej, M. (2006) Laminin α1 chain mediated reduction of laminin α2 chain deficient muscular dystrophy involves integrin α7β1 and dystroglycan. *FEBS Lett.*, **580**, 1759–1765.
50. Doe, J.A., Wuebbles, R.D., Allred, E.T., Ronney, J.E., Elorza, M. and Burkin, D.J. (2011) Transgenic overexpression of the α7 integrin reduces muscle pathology and improves viability in the dyW mouse model of merosin-deficient congenital muscular dystrophy type 1A. *J. Cell Sci.*, **124**, 2287–2297.
51. Kuang, S., Kuroda, K., Le Grand, F. and Rudnicki, M.A. (2007) Asymmetric self-renewal and commitment of satellite stem cells in muscle. *Cell*, **129**, 999–1010.
52. Kuang, S., Gillespie, M.A. and Rudnicki, M.A. (2008) Niche regulation of muscle satellite cell self-renewal and differentiation. *Cell Stem Cell*, **10**, 22–31.
53. Dumont, N.A., Wang, Y.X. and Rudnicki, M.A. (2015) Intrinsic and extrinsic mechanisms regulating satellite cell function. *Development*, **142**, 1572–1581.
54. Webster, M.T., Manor, U., Lippincott-Schwartz, J. and Fan, C.M. (2016) Intravital imaging reveals ghost fibers as architectural units guiding myogenic progenitors during regeneration. *Cell Stem Cell*, **4**, 243–252.
55. Chenette, D.M., Cadwallader, A.B., Antwine, T.L., Larkin, L.C., Wang, J., Olwin, B.B. and Schneider, R.J. (2016) Targeted mRNA decay by RNA binding protein AUF1 regulates adult

muscle stem cell fate, promoting skeletal muscle integrity. *Cell Rep*., **16**, 1379–1390.
56. Serrano, A.L., Baeza-Raja, B., Perdiguero, E., Jardí, M. and Munoz-Cánoves, P. (2008) Interleukin-6 is an essential regulator of satellite cell-mediated skeletal muscle hypertrophy. *Cell Metab*., **7**, 33–44.
57. Salerno, M.S., Dyer, K., Bracegirdle, J., Platt, L., Thomas, M., Siriett, V., Kambadur, R. and Sharma, M. (2009) *Akirin1* (*Mighty*), a novel promyogenic factor regulates muscle regeneration and cell chemotaxis. *Exp. Cell Res*., **315**, 2012–2021.
58. Halevy, O., Novitch, B.G., Spicer, D.B., Skapek, S.X., Rhee, J., Hannon, G.J., Beach, D. and Lassar, A.B. (1995) Correlation of terminal cell cycle arrest of skeletal muscle with induction of p21 by MyoD. *Science*, **267**, 1018–1021.
59. White, R.B., Biérinx, A.S., Gnocchi, V.F. and Zammit, P.S. (2010) Dynamics of muscle fibre growth during postnatal mouse development. *BMC Dev. Biol*., **10**, 21.
60. Tierney, M.T., Gromova, A., Sesillo, F.B., Sala, D., Spenlé, C., Orend, G. and Sacco, A. (2016) Autonomous extracellular matrix remodeling controls a progressive adaptation in muscle stem cell regenerative capacity during development. *Cell Rep*., **14**, 1940–1952.
61. Rossi, G., Antonini, S., Bonfanti, C., Monteverde, S., Vezzali, C., Tajbakhsh, S., Cossu, G. and Messina, G. (2016) Nfix regulates temporal progression of muscle regeneration through modulation of myostatin expression. *Cell Rep*., **14**, 1–12.
62. Snijders, T., Nederveen, J.P., McKay, B.R., Joanisse, S., Verdijk, L.B., van Loon, L.J. and Parise, G. (2015) Satellite cells in human skeletal muscle plasticity. *Front. Physiol*., **6**, 283.
63. Kuang, W., Xu, H., Vilquin, J.T. and Engvall, E. (1999) Activation of the *lama2* gene in muscle regeneration: abortive regeneration in laminin α2-deficiency. *Lab. Invest*., **7**, 1601–1613.
64. Kaufmann, M.H. (1992) *The Atlas of Mouse Development*. Academic Press, San Diego, CA, USA.
65. Rooney, J.E., Gurpur, P.B., Yablonka-Reuveni, Z. and Burkin, D.J. (2009) Laminin-111 restores regenerative capacity in a mouse model for α7 integrin congenital myopathy. *Am. J. Pathol*., **174**, 256–264.
66. Copp, A.J., Carvalho, R., Wallace, A., Sorokin, L., Sasaki, T., Greene, N.D. and Ybot-Gonzalez, P. (2011) Regional differences in the expression of laminin isoforms during mouse neural tube development. *Matrix Biol*., **30**, 301–309.
67. Bajanca, F., Luz, M., Duxson, M.J. and Thorsteinsdóttir, S. (2004) Integrins in the mouse myotome: developmental changes and differences between the epaxial and hypaxial lineage. *Dev. Dyn*., **231**, 402–415.
68. Paulsson, M. (1994) Biosynthesis, tissue distribution and isolation of laminins. In Ekblom, P. and Timpl, R. (eds), *The Laminins*. Harwood Academic Publishers, Amsterdam, pp. 1–26.
69. Gonçalves, A.B., Thorsteinsdóttir, S. and Deries, M. (2016) Rapid and simple method for in vivo ex utero development of mouse embryo explants. *Differentiation*, **91**, 57–67.
70. Rifes, P. and Thorsteinsdóttir, S. (2012) Extracellular matrix assembly and 3D organization during paraxial mesoderm development in the chick embryo. *Dev. Biol*., **368**, 370–381.
71. Preibisch, S., Saalfeld, S. and Tomancak, P. (2009) Globally optimal stitching of tiled 3D microscopic image acquisitions. *Bioinformatics*, **25**, 1463–1465.